

## NEW APPROACHES FOR THE NONLINEAR ASSESSMENT OF BUILDINGS SUBJECTED TO EARTHQUAKE AND TSUNAMI IN SEQUENCE

Camilo DE LA BARRA<sup>1</sup>, Tiziana ROSSETTO<sup>2</sup>, Crescenzo PETRONE<sup>3</sup>, Jorge VÁSQUEZ<sup>4</sup>

### ABSTRACT

Given the recent developments in computational tools to perform detailed nonlinear assessments of structures, analytical techniques appear to be a practical option to assess the structural performance of buildings under sequential earthquake and tsunami. This paper presents a comprehensive study for combinations of analysis methods that consider well established earthquake analysis techniques (nonlinear static pushover and response-history analyses), along with novel static and dynamic analysis methods to assess the structural response under tsunami inundation. The latter have been drawn on recent theoretical and experimental research regarding the characterisation of tsunami forces over buildings.

A 10 storey RC vertical evacuation building is assessed under combination of methods with differing computational complexity. The initial findings show that, for the assessed structure and assumptions considered, the use a nonlinear response history earthquake analysis, followed by a free vibration and a tsunami variable height pushover yields in excellent results in terms of global and local structural response when compared to fully dynamic analyses. Conversely, the use of simpler double pushover representation for the earthquake and the tsunami phases only results in a good prediction of the internal shear force in the critical elements, but in a significant bias in terms of the displacement response of the structure. It is seen that the appropriateness of this double pushover methodology for the cascading perils is intrinsically related to the appropriateness of the earthquake pushover to predict the structural behaviour under earthquake excitation, suggesting its use for more regular buildings.

*Keywords:* Tsunami engineering; Response-History Analysis; Pushover Analysis; Sequential Earthquake and Tsunami.

### 1. INTRODUCTION

Recent earthquake-triggered tsunamis have caused significant damage in coastal infrastructure and important life and economic losses, as the case of the 2011 Great East Japan Earthquake and Tsunami or the 2010 Maule Earthquake and Tsunami in Chile (e.g. Fraser et al. 2013, Kajitani et al. 2013 and Palermo et al. 2013). To improve the disaster resilience of coastal infrastructure subjected to these sequential hazards, it is crucial the development of risk assessment tools that can be used in the prediction of the impact of cascading earthquakes and tsunamis.

---

<sup>1</sup>Research Assistant, EPICentre, Department of Civil, Environmental and Geomatic Engineering, University College London (UCL), London, United Kingdom, [camilo.bustamante.16@ucl.ac.uk](mailto:camilo.bustamante.16@ucl.ac.uk)

<sup>2</sup>Professor, EPICentre, Department of Civil, Environmental and Geomatic Engineering, University College London, London, United Kingdom, [trossetto@ucl.ac.uk](mailto:trossetto@ucl.ac.uk)

<sup>3</sup>Earthquake Research Analyst, Willis Re, Willis Group Limited, London, United Kingdom, [Crescenzo.Petrone@WillisTowersWatson.com](mailto:Crescenzo.Petrone@WillisTowersWatson.com)

Research Assistant, National Research Center for Integrated Natural Disaster Management, Santiago, Chile, [jorge.vasquez@cigiden.cl](mailto:jorge.vasquez@cigiden.cl)

Despite the significant development in the modelling of earthquake and tsunami hazards (e.g. Goda et al. 2016, Suppasri et al. 2016), to date, the majority of the fragility studies that focus on the tsunami damage over infrastructure are empirically based (e.g. Mas et al. 2012, Charvet et al. 2014 and Suppasri et al. 2013). These studies are derived from field observations after significant events that have occurred in locations affected both by earthquakes and tsunamis. The main shortcomings of these empirical relationships are related to the fact that they are specific to the event and the building stock surveyed and they lack from locally measured tsunami intensity measures. Furthermore, in the case of earthquake-generated tsunamis, the observations within damaged assets after post-tsunami surveys usually cannot distinguish between earthquake and tsunami-related damage, and they are generally presented in the literature solely as tsunami fragility functions by neglecting the effect of the preceding earthquake damage (Charvet et al. 2017). Therefore, it is difficult to discriminate whether the preceding earthquake has significantly affected the structural performance under tsunami or not (Petrone et al. 2017).

### ***1.1 Previous studies on the assessment of structures under sequential earthquake and tsunami***

Very few studies assess the structural behaviour of buildings under the cascading effect of earthquake and tsunami. Among these, Park et al. (2012) developed fragility functions for a two-storey timber building subjected to successive earthquake and tsunami loading. They modelled the timber building as a single degree of freedom (SDoF) system, considering strength and stiffness degradation. Initially, earthquake nonlinear response history analyses were carried out for 44 ground motions. The structural model was then checked against collapse via tsunami pushover using a degraded backbone curve for the SDoF. A more complex approach and structural model was adopted by Latcharote and Kai (2014) in their assessment of the performance of a 7-storey reinforced concrete (RC) wall-frame structure under dynamic earthquake nonlinear response history analyses and subsequent tsunami pushover. However, both studies present limitations with regard to the representation of the tsunami loading, as they only consider constant height pushovers (CHPO) and use a coarse discretisation of the applied load along the height of the building (e.g. loads applied only at storey levels).

For tsunami only, Petrone et al. (2017) have proven that the representation and discretisation of the tsunami hydrodynamic loading play an important role in the reliability of the pushover analysis results. Petrone et al. (2017) looked at various structural analysis methods of differing complexity to assess the structural response of a RC frame under tsunami loading. They introduced the tsunami nonlinear response history analyses (TDY) and the variable height tsunami nonlinear pushover (VHPO), and they compared the reliability of these methods against the commonly used CHPO (e.g. Macabuag and Rossetto 2014, Attary et al. 2016). The characterisation of the tsunami forces over the assessed building was based in the research done by Qi et al. (2014).

Regarding these recent tsunami analysis methods, it is noted that TDY follows the same principles as an earthquake nonlinear response history analysis (denoted by DY in this paper). In TDY, a tsunami inundation height  $h(t)$  and velocity  $u(t)$  time history is used to calculate a corresponding lateral force time history  $F_T(t)$ . At each time step of the response history analysis, the tsunami force is applied to the structure assuming a triangular load distribution up to the tsunami inundation height at that time step, and the resulting structural response is measured. In terms of pushover-based approaches, the CHPO method is the most similar to a conventional earthquake pushover analysis (PO). In CHPO a constant inundation depth ( $h$ ) is considered, a lateral load pattern is applied to the structure following a triangular distribution, being the top displacement controlled throughout the analysis. By fixing the tsunami inundation height, an increase in the net lateral force means an increase in the flow velocity ( $u$ ), resulting in a variation in the Froude number ( $F_r$ ) associated with the tsunami inundation flow. VHPO analysis similarly applies lateral loads to the structure according to a triangular distribution, however it linearly increases the inundation depth up to a target value  $h_{max}$  (e.g. see Figure 1), whilst maintaining a constant Froude number. The VHPO is a force-controlled procedure, being the analysis more complex in comparison with CHPO which is a displacement-controlled analysis (Petrone et al. 2017). Due to this, VHPO analyses are not able to capture the post-peak behaviour in the pushover curve (e.g. branch D-E in Figure 1).

## 1.2 Objectives of this paper

Given the recent developments in computational tools to perform detailed nonlinear assessments of structures, analytical techniques appear to be a possible solution to assess the structural performance of buildings under sequential earthquake and tsunami. By using the same case-study building presented in Petrone et al. (2017) for tsunami only, this paper extends the study to include the preceding earthquake and unloading phases and compare the results of three methodologies of differing complexity.

## 2. NONLINEAR ANALYSIS METHODS TO ASSESS STRUCTURAL RESPONSE UNDER EARTHQUAKE AND TSUNAMI IN SEQUENCE

The approaches proposed to assess a structure under earthquake and tsunami combine different techniques to study the structural behaviour under the three phases involved, namely *earthquake* (EQ), *unloading* (UNL) until at-rest condition and *tsunami* (TS) phases. An illustrative example is presented in Figure 1, where the case of static earthquake pushover, free vibration unloading and tsunami variable-height pushover analysis combination (PO-FV-VHPO) is schematised. It is noted that the structural model should be capable to capture the damage accumulation throughout the analysis.

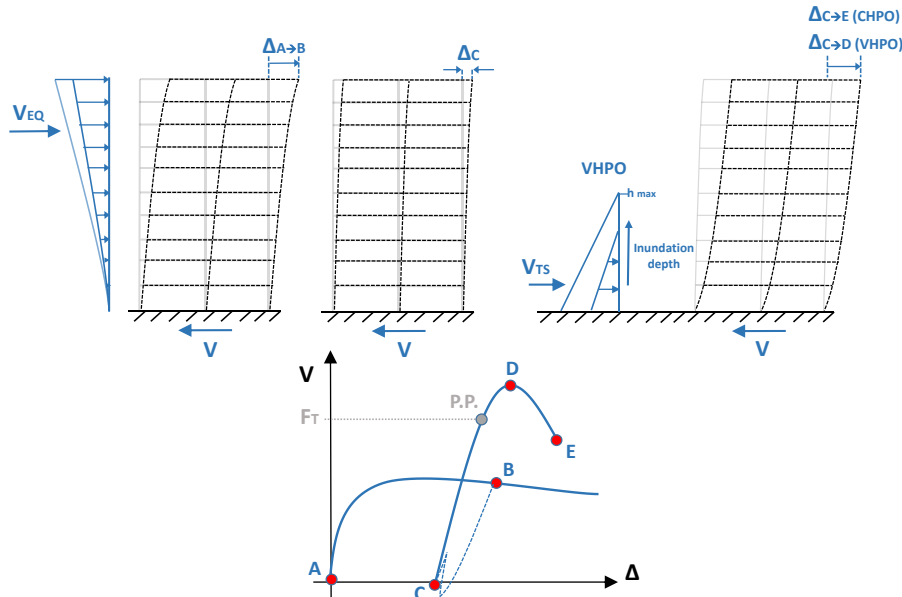


Figure 1. Schematic representation of the double pushover methodology for the PO-FV-VHPO case.

The earthquake loading phase can be represented either by a nonlinear response history analysis (DY) or by a static nonlinear pushover (PO) with a typical lateral load distribution following the shape of the first mode response of the structure (e.g. FEMA 2000). Several engineering response parameters (ERP) such as inter-storey drift ratios at each floor (IDR), top displacements, base shear, internal forces and floor accelerations can be measured in both analyses. In the case of pushover, the analysis needs to be stopped at a desired point (e.g. point B in Figure 1). This can be done until the attainment of a specific damage state associated to the achievement of a threshold value for the measured ERP(s), or, if a capacity spectrum based method is used (e.g. FRACAS, as per Rossetto et al. 2016), until the performance point derived for a given demand spectrum or ground motion record.

In the unloading phase (e.g. branch from point B to C in Figure 1) two approaches can be considered. The first is a transient free vibration analysis (FV), carried out over a time lapse enough to verify that the remaining base shear is zero and that the structure is fully at rest at the end of this phase. FV can be applied both following the earthquake DY and PO analyses. The second and simpler method is the static force-controlled approach (FC), this being only applicable after an earthquake pushover. In FC, the same earthquake pushover lateral load pattern at the end of the previous phase is kept constant, and an

increasing reverse lateral load pattern of mirrored shape is applied until a zero base shear is achieved. FC is a force-controlled analysis. In any case of unloading, if the structure has incurred in the nonlinear range during the earthquake excitation, a residual top displacement representing the *damaged* condition of the structure (e.g. point C in Figure 1) is expected to be present.

As discussed before, the tsunami impact can be assessed via either tsunami nonlinear response history analysis (TDY), constant height pushover (CHPO) and variable height pushover (VHPO); all of these analyses are fully detailed in Petrone et al. (2017). It is noted that due to its displacement-controlled formulation, only CHPO is capable of capturing the post-peak behaviour (e.g. trajectory D-E in Figure 1). On the other hand, in spite of not capturing the post-peak behaviour, VHPO is considered a more refined and realistic procedure than CHPO as it considers the variation of the inundation depth. For both pushover analyses, the performance point (P.P. in Figure 1) is determined at the point of intersection between the tsunami pushover curve and a horizontal line representing the external tsunami force demand  $F_T$ . The structure is assumed to be collapsed if the tsunami demand is larger than the structural capacity (i.e.  $F_T$  greater to global strength associated to point D in Figure 1). This definition of collapse relies on the fact that ductility does not play a significant role in the tsunami performance of the structure, as recently proven, albeit with significant assumptions, by Rossetto et al. (2018a).

It can be noted that the different combinations of techniques to assess the structural behaviour under each stage of the analysis yield in methodologies of varying complexity. Table 1 orders these methodologies in decreasing computational effort. Whilst a fully dynamic approach (DY-FV-TDY) may be computationally expensive, a simpler double pushover static approach (e.g. PO-FC-VHPO) is easier to implement but would results in more inaccurate results when compared to the former case. The final practitioner should be able to balance the computational effort and the accuracy required when selecting the most suitable method to assess the structure under sequential earthquake and tsunami.

Table 1. Different approaches to assess structural response under earthquake and tsunami in sequence.

Complexity	Earthquake (EQ)	Unloading (UNL)	Tsunami (TS)	ID
Decreasing ↓	Nonlinear Response History Analysis (DY)	Transient Free Vibration (FV)	Nonlinear Response History Analysis (TDY)	DY-FV-TDY
	DY	FV	Static Constant Height Pushover (CHPO)	DY-FV-CHPO
			Static Variable Height Pushover (VHPO)	DY-FV-VHPO
	Static Nonlinear Pushover Analysis (PO)	FV	CHPO	PO-FV-CHPO
			VHPO	PO-FV-VHPO
	PO	Static Force Controlled (FC)	CHPO	PO-FC-CHPO
			VHPO	PO-FC-VHPO

Among the possible approaches presented in Table 1, this paper focuses in assessing the results of DY-FV-VHPO and PO-FV-VHPO, when compared with the reference and more realistic DY-FV-TDY case. VHPO is selected instead of CHPO as it better captures the tsunami inundation and yields in better results when compared with TDY, as shown by Petrone et al. (2017). Verifications for the cases of force-controlled unloading procedure (FC) and tsunami CHPO are presented in Rossetto et al. (2018b).

### 3. APPLICATION CASE STUDY

#### 3.1. Case study building, numerical model and earthquake-tsunami time histories considered

A tsunami vertical evacuation building in Japan, corresponding to a 10-storey RC frame is used in this study. This same building has been used before by Petrone et al. (2017) to conduct a tsunami-only structural assessment. The reader is referred to that article for the detail of the geometrical and detailing characteristics of the structure. A 2D numerical model of an interior resisting plane of structure is developed in OpenSees (McKenna and Fenves 2013), considering a distributed plasticity approach with the use of the *nonlinearBeamColumn* element and 5 integration points per beam or column element. The OpenSees materials for the concrete and reinforcing steel are *Concrete04* and *Steel02* respectively. The mean material strengths for the concrete and reinforcing vary in accordance with the height, from 40 N/mm<sup>2</sup> in the lower three storeys to 27 N/mm<sup>2</sup> in the upper storeys. The steel characteristic strength corresponds to 390 N/mm<sup>2</sup> for the longitudinal reinforcing bars and 295 N/mm<sup>2</sup> for the transverse reinforcement. The column core is assumed as confined, leaving 5cm of unconfined cover concrete.

As seen in Figure 2, the masses (assumed value per unit area equal to 1.2 t/m<sup>2</sup>) are concentrated at the mid span of the interior beams. The tributary width for the frame is 6m. Considering the columns fixed at their base, the numerical model exhibits a fundamental period of 0.73s, and modal mass participation ratios of 77.9%, 12.2% and 4.5% for the first three modes of vibration. It is acknowledged that this structure would not be traditionally assessed under earthquake using a pushover approach, as its structural response would not be generally considered as first-mode dominated. However, it has been selected as a taxing candidate to test the accuracy of the selected combined methodologies (along with other assumptions made for the earthquake PO case), as its height is sufficient for it to withstand significant tsunami forces.

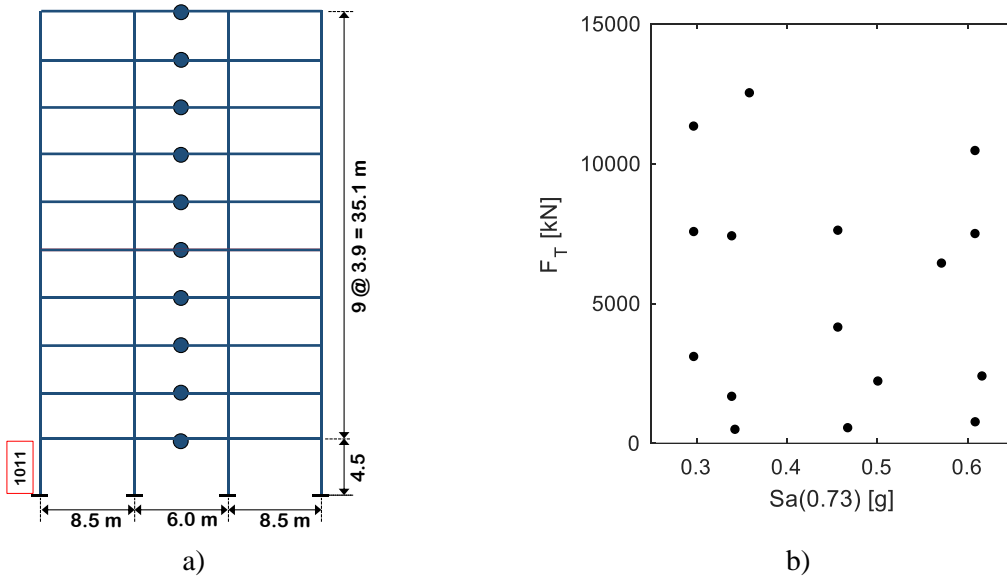


Figure 2. a) Numerical model of the building, with main dimensions and critical column 1011.  
b) Selected earthquake-tsunami (E-T) pairs used in this study, in terms of spectral accelerations  $Sa(0.73)$  for each ground motion record and the tsunami peak force ( $F_T$ ) for each wave trace.

A set of 16 coherent earthquake ground motions and tsunami wave traces (E-T pairs) is considered as per Figure 2b (refer to Table 2 in the Appendix of this paper for more detail of the records characteristics). These pairs were selected from the work done by Goda et al. (2016), who simulated ground motion time histories for the 2011 Japan Earthquake using a multiple-event stochastic finite-fault method, being the resulting tsunami wave traces obtained through multiple realisations of wave profiles in which the nonlinear shallow water equations with run-up were evaluated.

It is noted that for each tsunami wave trace, the tsunami force  $F_T(t)$  is determined using the expressions given by Qi et al. (2014), which give an estimation of the forces on partially immersed rectangular bodies in quasi-steady flows. The use of this formula assumes that a steady-state flow is representative

of the tsunami inundation. This assumption has been shown to be reasonable by Foster et al. (2017). The tsunami peak force  $F_T$  corresponds to the maximum value of  $F_T(t)$ . According to Qi et al. (2014), the tsunami force  $F_T(t)$  per unit of width can be estimated as per Equation 1:

$$\frac{F_T(t)}{b} = \text{sgn}(u) \left\{ \begin{array}{ll} 0.5 C_D \rho u^2 h & \text{if } F_r < F_{rc} \\ \lambda \rho g^{\frac{1}{3}} u^{\frac{4}{3}} h^{\frac{4}{3}} & \text{if } F_r \geq F_{rc} \end{array} \right. \quad (1)$$

In which  $C_D$  is the drag coefficient,  $\rho$  is the sea water density ( $1,200 \text{ kg/m}^3$ ),  $\text{sgn}(u)$  is the sign function of the flow velocity,  $g$  is the acceleration of gravity,  $\lambda$  is the choking ratio.  $F_r = u/\sqrt{g \cdot h}$  is the Froude number and  $F_{rc}$  is the Froude number threshold, which denotes subcritical ( $F_r < F_{rc}$ ) and choked ( $F_r \geq F_{rc}$ ) conditions for the steady-state flow.  $F_{rc}$ ,  $C_D$  and  $\lambda$  are dependent on the blocking ratio parameter  $b/w$  (Qi et al. 2014). A blocking ratio of 0.6 is assumed in this paper, with corresponding values of  $C_D=4.7$ ,  $\lambda=2.0$  and  $F_{rc}=0.32$ .

### 3.2. Earthquake loading, unloading and tsunami loading stages

In the case of the static earthquake pushover, in order to eliminate the effect of estimation errors in the earthquake performance point arising from, for instance, the use of a capacity spectrum based assessment, it is decided in this paper to use the maximum inter-storey drift ratio from the DY analysis ( $IDR_{max, DY}$ ) to define the performance point at the corresponding PO analysis. Each PO analysis is stopped when an  $IDR$  value equal to  $IDR_{max, DY}$  is reached, at the same storey at which it was observed in the DY analysis. It is acknowledged that this matching procedure would lead to different estimates of the overall damage distribution on the structure (with the exception of the damage state at the matched floor), as for the assessed structure, the response under dynamic excitation differs from the response under static pushover. Hence, the  $IDR$  values in PO along the “non-matched” storeys may be significantly different to  $IDR_{max, DY}$  from the dynamic case. In fact, for some response cases, the IDR profiles between DY and PO are different, being the  $IDR_{max, DY}$  values reached at the upper storeys in the case of DY, whereas PO predicts the occurrence of the maximum inter storey drift ratio ( $IDR_{max}$ ) at the mid-height of the building.

For earthquake PO, the lateral load pattern follows the shape fundamental mode of the structure. Displacement increments of 2/10,000 times the building height are considered. On the other hand, the nonlinear response history analyses (DY) consider a Newmark integrator with  $\gamma=0.5$  and  $\beta=0.25$  and a damping ratio of  $\zeta=5\%$ . In case of convergence issues, the integration time step is conveniently reduced. Following the earthquake stage (either DY or PO), the dynamic free-vibration unloading procedure, FV, is carried out over a time lapse of 10s, assuming a higher damping ratio of  $\zeta = 30.0\%$  and using a Newmark integrator with the same previously defined parameters. It is corroborated that at the end of this stage the structure is at rest condition.

Finally, the analyses characterising the tsunami loading phase (TDY and VHPO) are performed assuming triangular load distributions, with 5 discrete loads per storey applied at the left-hand side of the structure (see Figure 2a). This discretisation is based on the results shown by Petrone et al. (2017), given the good balance between accuracy and computational effort. The dynamic parameters to analyse the structure under TDY are the same as in the earthquake case, also with reduction of the time step in case of convergence issues. For the VHPO analyses, the inundation depth is varied from 0 m up to a maximum value of  $h^{max}$  of 21 m, considering 300 increments. When VHPO is compared to TDY, the equivalent VHPO analyses are performed at a constant Froude number,  $F_r^{peak}$ , equal to the Froude number value obtained when the peak tsunami force ( $F_T$ ) is achieved in the corresponding tsunami wave trace. VHPO uses a force-controlled integrator.

## 4. COMPARISON OF THE SELECTED APPROACHES

This section presents the comparison of the results obtained by three different methodologies used to

assess the structural response under sequential earthquake and tsunami impact. As mentioned in Section 2, the reference case is the fully dynamic analysis (DY-FV-TDY), which is considered the most realistic and complex methodology. It is noted that DY-FV-TDY is capable to capture the dynamic response of the structure under the ground motions and corresponding wave traces. To study how the simplification in the tsunami loading affects the overall response, TDY is changed to VHPO and the results are compared. Finally, to determine the effect on the structural response by introducing the simplification in the earthquake loading phase, along with the assumptions described in Section 3.2, PO-FV-VHPO is studied. The comparisons consider the structural response in terms of the global behaviour (base shear versus top displacement), IDR distribution and shear internal force the most critical column under tsunami (1011, as per Figure 2a).

#### 4.1. The reference case (DY-FV-TDY)

The DY-FV-TDY analyses are carried out for the 16 E-T pairs presented in Figure 2b. Figure 3 shows the resulting force-displacement response histories and the IDR profiles at the point of maximum demand (i.e. maximum top displacement). The responses for the pairs E-T-21 ( $S_a(0.73 \text{ s}) = 0.572g$ ,  $F_T=6,411 \text{ kN}$ ) and E-T-11 ( $S_a(0.73 \text{ s}) = 0.617g$ ,  $F_T=2,373 \text{ kN}$ ) are plotted. These pairs have been selected among the suite of E-T records as representative cases of similar earthquake excitation levels with different tsunami intensities. It is noted that for clarity, the graphs only show the tsunami final responses. The effect of the preceding earthquake is evident from the tsunami pushover curves starting from a non-zero residual deformation.

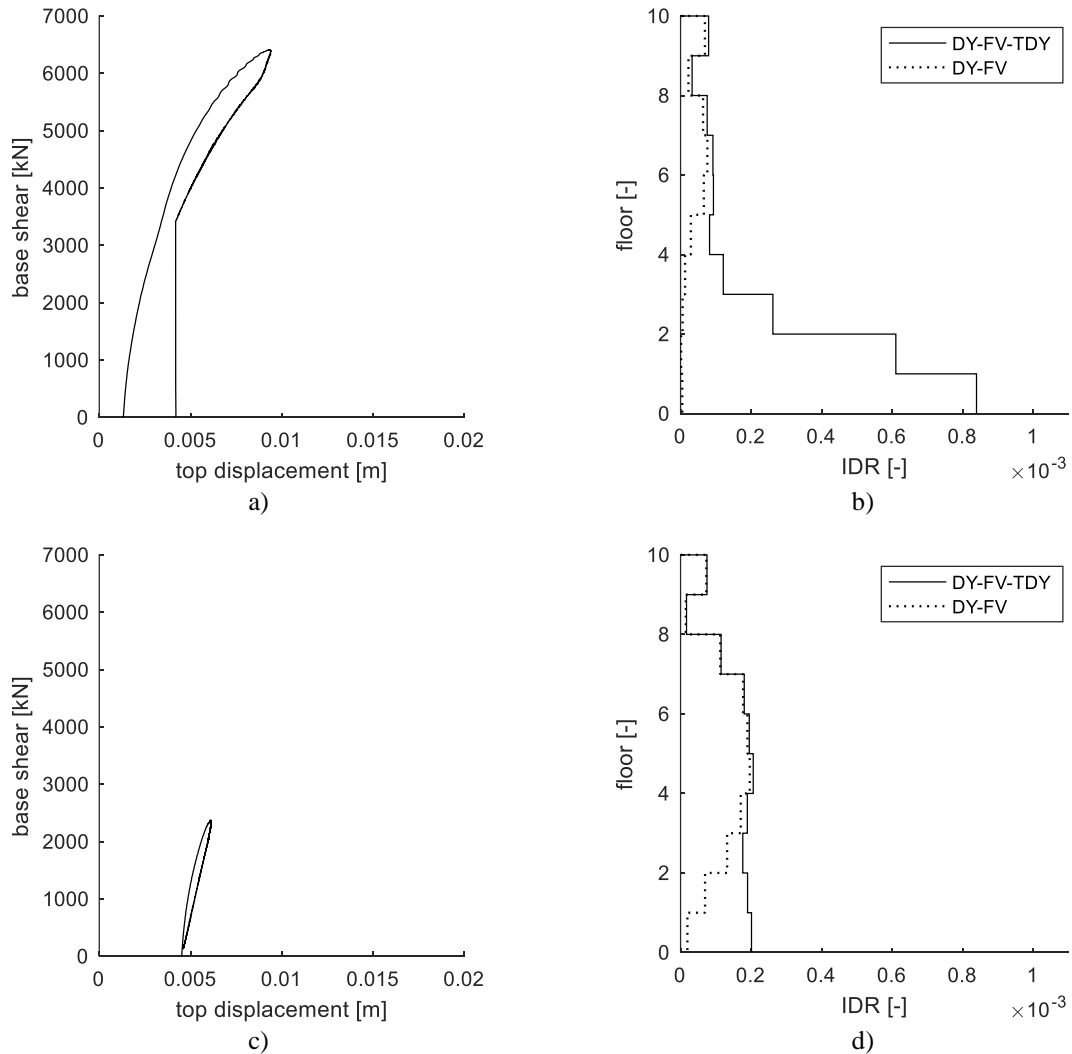


Figure 3. Response histories for E-T-21 (top) and E-T-11 (bottom).

(a) and (c) base shear-top displacement tsunami envelopes; (b) and (d) tsunami IDR at maximum demand.

Figure 3b and 3d also present the residual IDR profile after the earthquake and free vibration phases (labelled as ‘DY-FV’). From both illustrated cases, it is clear that the earthquake induces higher residual IDRs in the mid-height of the building. When the tsunami peak force intensity is moderate to large, the IDR profile is substantially modified at lower storeys in where the tsunami loading is applied. For the middle and upper storeys, the tsunami loading does not substantially modify the residual deformation after the occurrence of the earthquake. Also, it is noted that for some earthquakes within the suite,  $IDR_{max, DY}$  occurs in the upper storeys. Again in those cases, it is seen that when the tsunami intensity is relatively large, the damage distribution shifts to the lower storeys.

#### 4.2. Comparisons between the reference case and DY-FV-VHPO and PO-FV-VHPO

Figure 4 presents the comparisons of the results between DY-FV-TDY, the reference case, and DY-FV-VHPO and PO-FV-VHPO in terms of global response (base shear versus top displacement) and IDR ratios at the performance point in the case of the tsunami pushovers. It is recalled that the performance points (red and green dots in Figure 4) are obtained from the intersection between the tsunami pushover curve and a horizontal line representing the peak force of the corresponding wave trace. The results correspond to the same E-T pairs shown in the previous section.

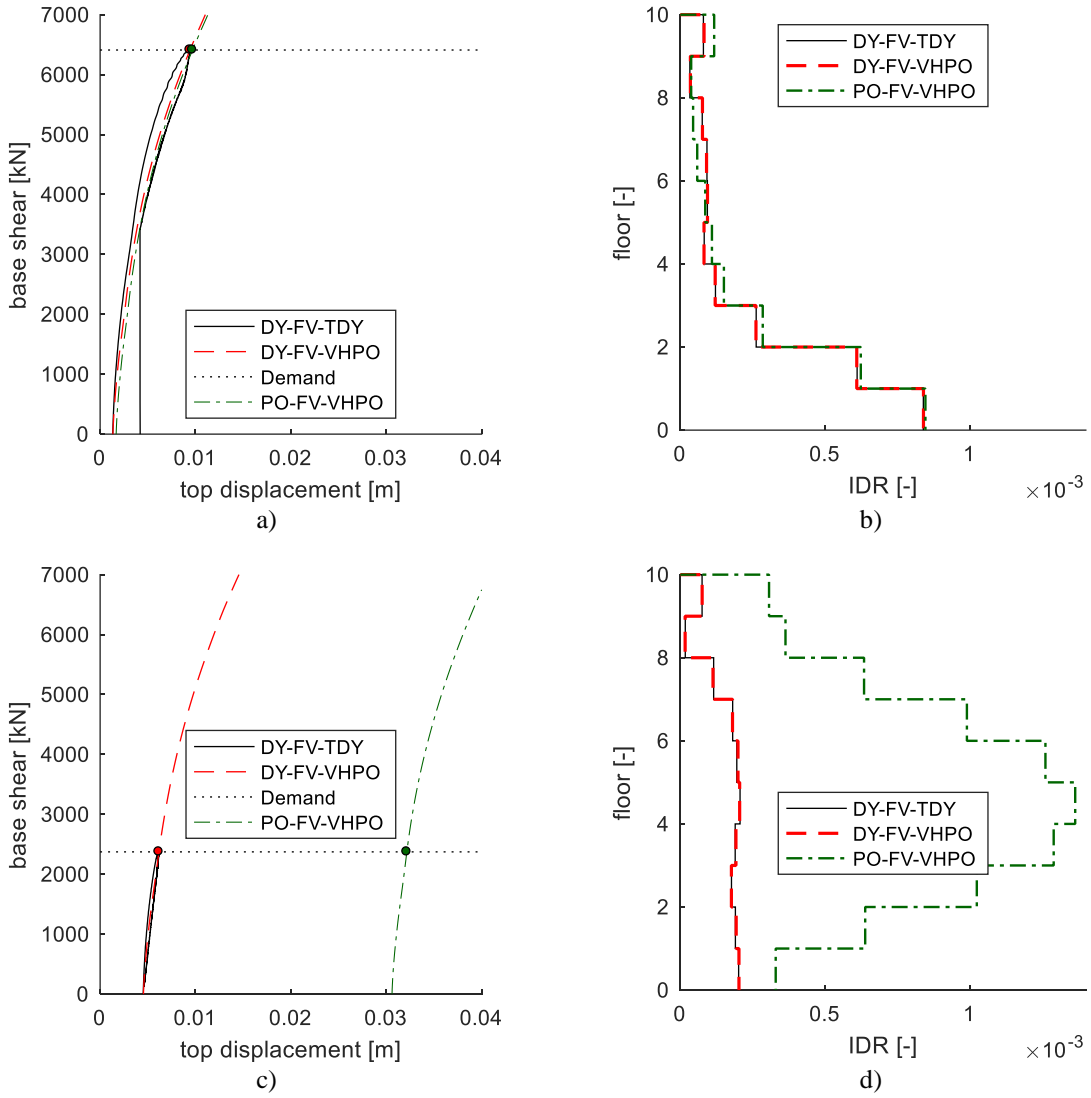


Figure 4. Response histories for E-T-21 (top) and E-T-11 (bottom). Comparison between DY-FV-TDY and DY-FV-VHPO / PO-FV-VHPO analyses. (a) and (c) base shear- top displacement tsunami envelopes; (b) and (d) tsunami IDR profiles.

For both E-T pairs shown, it is noted that the agreement between DY-FV-TDY and DY-FV-VHPO

analyses is very good. The global loading curve of VHPO predicts reasonably well the behaviour of the structure under TDY up to the demand level, and the difference between the IDR profiles is quite negligible. On the other hand, the change in the analysis type in the earthquake phase (i.e. from DY to PO), leads to a worse estimation in the global displacements and IDR distributions at the tsunami performance points, particularly significant in the case of E-T-11. For E-T-21, unloading from the pushover curve at  $IDR_{max} = 0.367\%$  yields in a similar but slightly larger residual displacement than the DY case which in turn results in a similar estimation of the tsunami global response and IDR profiles. Conversely, the ground motion associated to E-T-11 induces a much higher  $IDR_{max, DY} = 0.670\%$ . This results in a significant residual displacement after the PO-FV phases for E-T-11 when compared with E-T-21 (see Figure 2a and 2c). This large residual displacement (which is further expressed in a large shift of the tsunami pushover curve along the horizontal axis) is not observed in the corresponding DY-FV-VHPO case. As for this particular case of E-T-11, given that the tsunami intensity is relatively low, the tsunami pushover does not substantially modify the residual IDR profile resulting from the earthquake PO analysis. Hence, for E-T-11, the final IDR profile in the PO-FV-VHPO analysis is significantly different from the one obtained using DY-FV-TDY. This discrepancy is observed for the cases where the earthquake pushover, given the “matching procedure” assumption used in this paper, significantly pushes the structure within the nonlinear range and the subsequent tsunami intensity is relatively low.

Figure 5 illustrates the performance of DY-FV-VHPO and PO-FV-VHPO in predicting the ground storey IDR ( $IDR_1$ ) and the shear internal force in the most loaded column under tsunami (1011), when compared to the DY-FV-TDY reference case for the 16 E-T pairs used. The horizontal axis in Figure 5 corresponds to the peak tsunami force achieved in the corresponding wave trace (which equals the maximum base shear sustained by the structure). With respect to the estimation of  $IDR_1$ , it is clear that the introduction of the earthquake pushover method along with the assumptions made in Section 3.2, makes the PO-FV-VHPO methodology the worse estimator, especially for the range of lower tsunami peak forces in where the tsunami does not have a significant influence (e.g.  $F_T < 2,000$  kN, as seen in Figure 5a).

Despite these differences in the IDR responses when using earthquake PO instead of DY analysis, PO-FV-VHPO predicts reasonably well the shear internal force in the most critical column of the structure, at the tsunami performance point (Figure 5b). This is explained as the shear internal force at the ground storey of the building is driven by the tsunami loading; observation which is sustained by the lack of significant difference in shear internal force values when the earthquake analysis type is changed. Whereas the most accurate DY-FV-VHPO methodology underestimates the internal shear force by up to 3%, PO-FV-VHPO gives a reasonable underestimation up to 4% and two cases where the overestimation does not exceed 2% (Figure 5b). When the tsunami peak force increases, both methodologies yield more accurate estimates of the shear internal force at the critical column.

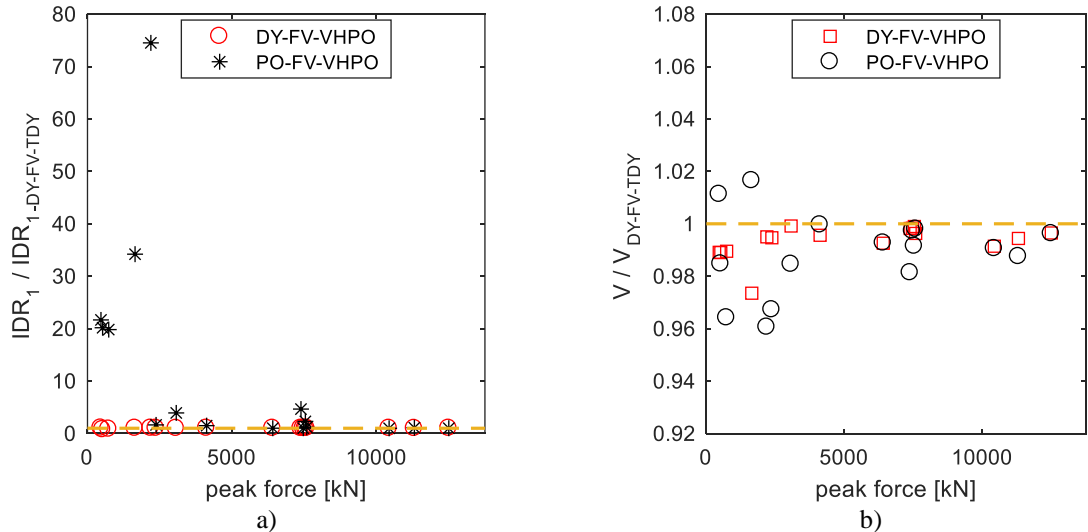


Figure 5. Error in the estimation of  $IDR_1$  and shear force in column 1011 at the performance point under tsunami. Comparison between DY-FV-VHPO / PO-FV-VHPO methods against the reference DY-FV-TDY case.

For the assessed building, the DY-FV-VHPO methodology has proven to be the best predictor of the structural response under earthquake and tsunami in sequence. It is evident that the use of PO has an important effect on the overall response under sequential earthquake and tsunami. This is particularly related to the significant differences between earthquake DY and PO in terms of the prediction of the deformed shape and damage concentration on the structure. Given these observations, the use of earthquake PO analysis would not be recommended to assess the earthquake-tsunami behaviour of the case study structure, as this structure does not present a behaviour suitable to be analysed under a traditional pushover.

## 5. CONCLUSIONS

This paper presents a comparison of three novel methodologies to assess the structural response under sequential earthquake and tsunami. The results from the most accurate and computationally complex DY-FV-TDY case, are compared against variations in the analysis methods for the earthquake and tsunami loading phases, with decreasing computational effort: DY-FV-VHPO and PO-FV-VHPO. From the observed results, considering that various assumptions have been made and only a single 2D structure has been studied, the following conclusions can be drawn:

- 1) The DY-FV-VHPO methodology yields in very good predictions of the global and local structural behaviour at the tsunami performance point, when compared to the reference case. This suggests the use of this methodology in the assessment of critical and complex infrastructure (e.g. tall and/or irregular buildings) under sequential earthquake and tsunami, providing a reasonable balance between computational effort and accuracy of the results. It is noted that the advantage of this method, in comparison with DY-FV-TDY, relies on the fact that the analysis can be performed under several tsunami intensity levels without the necessity of having site-specific tsunami inundation time-histories.
- 2) For the case study structure and the assumptions considered, the PO-FV-VHPO methodology only presents reasonable predictions of the shear internal force in the most critical column under tsunami. The IDR profiles at the tsunami performance point are not well predicted, these being significantly influenced by the determination of the performance point at the earthquake pushover curve. This suggests that the PO-FV-VHPO methodology, simpler and easier to implement than DY-FV-TDY, may be appropriate only in the cases where a PO approach is appropriate to assess the structural performance under the earthquake loading. Examples of

these cases are related to regular structures with first-mode dominated behaviour under earthquake loading. Due to its simplicity, the double pushover methodology may be suitable for fragility assessments of populations of buildings presenting these characteristics.

These conclusions will be confirmed by applying the presented methodologies to other types of structures (e.g. regular and shorter buildings). Further work is also related with the study of the effect of other components of the tsunami loading on the final response of the structure. These include the impulsive loads, debris impact and buoyancy forces.

## 6. ACKNOWLEDGMENTS

The research presented in this paper has been predominantly funded by the European Research Council under the European Union's Seventh Framework Programme (FP7/2007–2013)/ERC grant agreement number 336084 ‘URBANWAVES’, awarded to Professor Tiziana Rossetto. We also thank Willis Re for supporting the time of Dr. Petrone for this research.

## 7. REFERENCES

- Attary, N.van de Lindt, J. W.Unnikrishnan, V. U.Barbosa, A. R.and Cox, D. T. (2017) ‘Methodology for Development of Physics-Based Tsunami Fragilities’, *Journal of Structural Engineering*, 143(5).
- Charvet, I.Ioannou, I.Rossetto, T.Suppasri, A.and Imamura, F. (2014) ‘Empirical fragility assessment of buildings affected by the 2011 Great East Japan tsunami using improved statistical models’, *Natural Hazards*, 73(2), pp. 951–973.
- Charvet, I.Macabuag, J.and Rossetto, T. (2017) ‘Estimating Tsunami-Induced Building Damage through Fragility Functions: Critical Review and Research Needs’, *Frontiers in Built Environment*, 3(36).
- FEMA (2000) *FEMA 356. Prestandard and Commentary for the Seismic Rehabilitation of Buildings*. Washington.
- Foster, A. S. J.Rossetto, T.and Allsop, W. (2017) ‘An experimentally validated approach for evaluating tsunami inundation forces on rectangular buildings’, *Coastal Engineering*, 128(2017), pp. 44–57.
- Fraser, S.Raby, A.Pomonis, A.Goda, K.Chian, S. C.Macabuag, J.Offord, M.Saito, K.*et al.* (2012) ‘Tsunami damage to coastal defences and buildings in the March 11th 2011 Mw9.0 Great East Japan earthquake and tsunami’, *Bulletin of Earthquake Engineering*, 11(1), pp. 205–239.
- Goda, K.Petrone, C.de Risi, R.and Rossetto, T. (2017) ‘Stochastic coupled simulation of strong motion and tsunami for the 2011 Tohoku, Japan earthquake’, *Stochastic Environmental Research and Risk Assessment*, 31(9), pp. 2337–2355.
- Kajitani, Y.Chang, S. E.and Tatano, H. (2013) ‘Economic Impacts of the 2011 Tohoku-Oki earthquake and tsunami’, *Earthquake Spectra*, 29(SUPPL.1), pp. S457–S478.
- Latcharote, P. and Kai, Y. (2014) ‘Nonlinear Structural Analysis of Reinforced Concrete Buildings Suffering Damage from Earthquake and Subsequent Tsunami’, in *10th U.S. National Conference on Earthquake Engineering - Frontiers of Earthquake Engineering*.
- Macabuag, J.Lloyd, T.and Rossetto, T. (2014) ‘Towards the Development of a Method for Generating Analytical Tsunami Fragility Functions’, in *Second European Conference on Earthquake Engineering and Seismology*.
- Mas, E.Koshimura, S.Suppasri, A.Matsuoka, M.Matsuyama, M.Yoshii, T.Jimenez, C.Yamazaki, F.*et al.* (2012) ‘Developing Tsunami fragility curves using remote sensing and survey data of the 2010 Chilean Tsunami in Dichato’, *Natural Hazards and Earth System Science*, 12(8), pp. 2689–2697.
- McKenna, F. and Fenves, G. (2013) *OpenSees Manual*. Berkeley, California. Available at: <http://opensees.berkeley.edu>.
- Palermo, D.Nistor, I.Saatcioglu, M.and Ghobarah, A. (2013) ‘Impact and damage to structures during the 27 February 2010 Chile tsunami’, *Canadian Journal of Civil Engineering*, 40(8), pp. 750–758.
- Park, S.van de Lindt, J. W.Cox, D.Gupta, R.and Aguiniga, F. (2012) ‘Successive Earthquake-Tsunami Analysis to Develop Collapse Fragilities’, *Journal of Earthquake Engineering*, 16(6), pp. 851–863.

Petrone, C.Rossetto, T.and Goda, K. (2017) ‘Fragility assessment of a RC structure under tsunami actions via nonlinear static and dynamic analyses’, *Engineering Structures*. The Authors, 136, pp. 36–53.

Qi, Z. X.Eames, I.and Johnson, E. R. (2014) ‘Force acting on a square cylinder fixed in a free-surface channel flow’, *Journal of Fluid Mechanics*, 756, pp. 716–727.

Rossetto, T.Gehl, P.Minas, S.Galasso, C.Duffour, P.Douglas, J.and Cook, O. (2016) ‘FRACAS: A capacity spectrum approach for seismic fragility assessment including record-to-record variability’, *Engineering Structures*, 125, pp. 337–348.

Rossetto, T.De la Barra, C.Petrone, C.and De la Llera, J. C. (2018b) ‘Comparison of Nonlinear Static and Dynamic Analysis Methods for Assessing Structural Response Under Earthquake and Tsunami in Sequence (submitted)’, *Earthquake Engineering and Structural Dynamics*.

Rossetto, T.Macabuag, J.Petrone, C.and Eames, I. (2018a) ‘Does Ductility Play a Significant Role in the Response of Structures to Tsunami Loading ? (under review)’, *Earthquake Spectra*.

Suppasri, A.Latcharote, P.Bricke, J. D.Leelawat, N.Hayashi, A.Yamashita, K.Makinoshima, F.Roeber, V.*et al.* (2016) ‘Improvement of Tsunami Countermeasures Based on Lessons from The 2011 Great East Japan Earthquake and Tsunami — Situation After Five Years’, *Coastal Engineering Journal*, 58(4), p. 1640011.

Suppasri, A.Mas, E.Charvet, I.Gunasekera, R.Imai, K.Fukutani, Y.Abe, Y.and Imamura, F. (2013) ‘Building damage characteristics based on surveyed data and fragility curves of the 2011 Great East Japan tsunami’, *Natural Hazards*, 66(2), pp. 319–341.

## 8. APPENDIX

Table 2 summarises the characteristics of the earthquake-tsunami pairs used in this study. All the ground motion records have a duration of 140 s.

Table 2. Earthquake-tsunami pairs used in this paper.

E-T pair ID	PGA (g)	Sa(0.73 s) (g)	F <sub>T</sub> (kN)	h at F <sub>T</sub> (m)	u at F <sub>T</sub> (m/s)	Fr <sup>peak</sup> at F <sub>T</sub>	TS duration (s)
E-T-01	0.433	0.609	734.930	2.460	-4.330	0.882	425
E-T-05	0.552	0.457	4122.164	5.760	-6.740	0.897	597
E-T-08	0.952	0.344	466.303	3.250	-2.330	0.413	362.5
E-T-15	0.806	0.298	3071.122	11.220	-3.180	0.303	372
E-T-19	0.250	0.609	7467.409	8.660	-7.000	0.760	205
E-T-21	0.321	0.572	6410.927	8.820	-6.130	0.659	229
E-T-11	0.274	0.617	2373.426	5.280	-4.860	0.675	630.5
E-T-17	0.806	0.298	7538.810	9.510	-6.420	0.665	473
E-T-20	0.552	0.457	7586.031	9.280	-6.610	0.693	261.5
E-T-23	1.130	0.340	7386.874	11.790	-5.100	0.474	617
E-T-25	1.130	0.340	1646.138	7.170	-2.720	0.324	471
E-T-10	0.632	0.502	2192.915	5.410	-4.470	0.614	422.5
E-T-02	0.559	0.468	523.300	2.780	-2.970	0.569	583.5
E-T-27	0.694	0.360	12501.695	13.140	-6.790	0.598	529.5
E-T-28	0.916	0.298	11310.648	12.030	-6.880	0.633	446.5
E-T-29	0.250	0.609	10437.033	12.650	-6.160	0.553	201